Vol. 44, No. 3 (2022) 482-497, DOI: 10.24874/ti.1286.04.22.07

Tribology in Industry

www.tribology.rs

RESEARCH

# Design of Hydrodynamically Lubricated a New Micro-pocketed Tilting Pad Thrust Bearing Based on Simulated Performance Parameters

J.C. Atwal[a,*] and R.K. Pandey[a]

[a]*Department of Mechanical Engineering, IIT Delhi, New Delhi-110016, India.*

Keywords:

*Thrust bearings*
*Tilting pad*
*Micro-pockets*
*Numerical simulations*
*Bearing design*

**Corresponding author:*

*Jeewan C. Atwal*
*E-mail: jeewanatwal49@gmail.com*

*Received: 14 April 2022*
*Revised: 8 June 2022*
*Accepted: 9 July 2022*

A B S T R A C T

*Numerical investigation has been performed at several operating parameters for developing the graphs to design a hydrodynamically lubricated new micro-pocketed tilting pad thrust bearing. The performance parameters (minimum film thickness, friction coefficient, inflow, side leakage, and dynamic coefficients i.e., stiffness and damping) with new micro-pocketed pad have been plotted as a function of pivot location. The use of these graphs has been demonstrated by presenting a solved design problem. The performance parameters of bearings achieved with the new micro-pocketed pad have been compared with plain and rectangular micro-pocketed pads at wide range of operating parameters. With the new micro-pocketed pad, up to 37.4% & 7.7% increase in the minimum film thickness and 14.3% & 7% reduction in friction coefficient have been found compared to the plain and existing rectangular shape pocketed pads, respectively.*



## 1. INTRODUCTION

Fluid film tilting pad thrust bearings are widely employed in centrifugal compressors, hydraulic and steam turbines, vertical turbine pumps, large size helical gearboxes etc. to efficiently support and guide the axially loaded rotors. To avoid expensive and time-consuming designs of plain tilting pad thrust bearings by solving the coupled governing equations iteratively, researchers have developed and presented the design charts in the past [1,2]. It is worth mentioning here that since recent past, the surface texture has emerged as a viable technology for addressing the tribo-dynamic concerns of machine contacts. Surface texture involves presence of tiny micro/nano dimples, micro-grooves, and micro-pockets at the tribo-components at the optimum locations for achieving the best performances. Thus, exploring and enhancing the performances of tilting pad bearings employing new conceived surface textures are vital research task.

In the past, researchers have demonstrated that different tailored surface textures can substantially improve the bearings' performances [3-13]. The advancement in manufacturing technologies have enabled the

creation of tiny micro-structures of different shapes and sizes, leading to the development of tailored textures on pad surfaces [14]. It has been understood that when the plain runner surface interfaces with the textured bearing surface in the presence of lubricant at favorable operating parameters, numerous micro-hydrodynamic bearings get formed, which sustains the applied external load energy efficiently [15-17]. In addition to this, the micro/tiny geometries present in the texture act as innumerable lubricant reservoirs, which trap the wear debris and contaminants [18-20]. This mainly reduces three-body abrasion in the mixed and boundary lubrication regimes at the time of start and stop of runner/rotor. The investigators have also attempted to enhance the performance of bearings by optimizing the shape and size of micro/nano geometries of the textures [4, 21-28]. Furthermore, the influences of the number of dimples [29], the area density of dimples [7,30-32], geometric shape of dimples [33-34] and dimple sizes [35-37] etc. have also been investigated on the performances of the bearings and tribo-pairs. It has been found that the area density of dimples falling in the range of 5–13% has produced beneficial tribo-results [32].

The researchers have also investigated tapered land, close rectangular micro-pocket, open micro-pocket, and textured pad bearings using CFD-based simulations [38]. It has been concluded that the open rectangular micro-pocket bearing performed better as compared to other adopted configurations. The authors have explored the effect of cross-sectional shapes (square, circular, trapezoidal, and triangular) of micro-grooves on the performance of thrust bearing, and it has been found that the micro-grooves having square cross-section performed the best among all the considered cases [39]. In a recent publication on tilting pad bearings, the investigators employed four different configurations of pads, namely rectangular micro-pocketed pad, radial grooved pad, circumferentially grooved pad, and rectangular dimpled pad. The performance computation of these bearings using CFD simulations has revealed that the rectangular-micro-pocketed pad performed better as compared to other pad designs [40].

Literature review revealed that the rectangular micro-pocketed pads have performed better as compared to the plain, profiled [41-43], micro-grooved, and textured (square dimples) tilting pad thrust bearings operating with thin film under hydrodynamic lubrication regime. This motivated the present authors to conceive new micro-pocketed tilting pad based on the numerical exploration for further improving the performance parameters as compared to rectangular micro-pocketed case. Therefore, the objective of this paper is set to conceive a new high performing micro-pocketed tilting pad based on numerical simulation considering the hydrodynamic lubrication regime. Moreover, the main objective of this paper is to present graphs for use in rapid design of the new conceived micro-pocket tilting pad.

## 2. GEOMETRICAL DESCRIPTION OF BEARING PADS AND GOVERNING EQUATIONS

Figures 1(a) and 1(b) show the 3D-CAD diagram of the tilting (pivoted) pad thrust bearing and coordinate system employed. Figures 2(a) and 2(b) present the top and front sectional views of plain and new micro-pocketed pads.

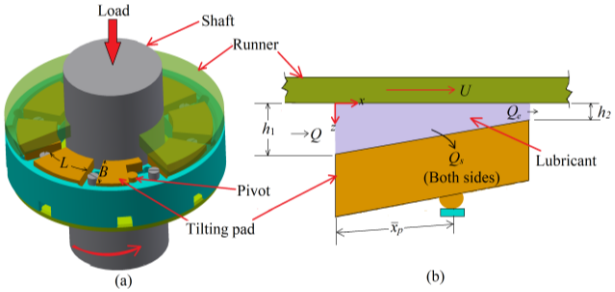


**Fig. 1**. (a) Schematic CAD model of a tilting pad thrust bearing system, (b) Sketch of a tilting pad interfaced with a runner segment with co-ordinate system.

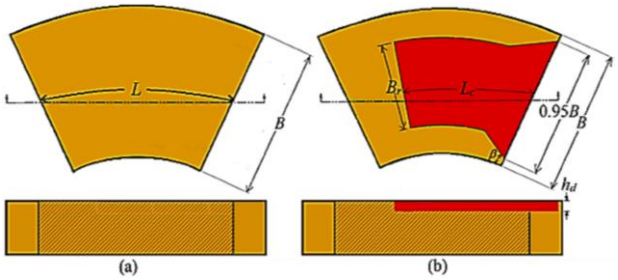


**Fig. 2.** (a) Top and front (section) views of conventional (plain) tilting pad, (b) Top & front (section) views of new micro-pocketed tilting pad.

The design graphs have been developed for finding the performance parameters minimum film

thickness, load-carrying capacity, friction force, inflow, side leakage, bearing dynamic coefficients etc. Equations (1)-(9) have been employed for computing the performance parameters. The pressures at the grids in the domain have been achieved by the solution of the governing Reynolds equation. The discretisation of this equation has been done using the FEM (finite element method), as explained in the coming sub-section 2.1.

The dimensionless film load carrying capacity per pad is found by the following equation:

$$\bar{W} = \frac{m^2}{\eta_0 UB} W = \int_0^1 \int_0^1 \bar{p}\, d\bar{x} d\bar{y} \tag{1}$$

The dimensionless minimum film thickness is written below:

$$\bar{h}_2 = h_2/(Lm) = 1/((h_1/h_2)-1) \tag{2}$$

The dimensionless expressions used for finding the friction force ( $\bar{F}$ ), flow rate ( $\bar{Q}_i$ ), and side leakage ( $\bar{Q}_s$ ) are provided below:

$$\bar{F} = \frac{m}{\eta_0 ULB} F = \int_0^1 \int_0^1 \left( \frac{\bar{\eta}}{\bar{h}} + 0.5\bar{h} \frac{\partial \bar{p}}{\partial \bar{x}} \right) d\bar{x} d\bar{y} \tag{3}$$

$$\bar{Q}_i = \frac{Q_i}{ULm} = \int_0^1 \left( -\frac{d\bar{p}}{d\bar{x}} \frac{\bar{h}^3}{12\bar{\eta}} + 0.5\bar{h} \right) d\bar{y} \tag{4}$$

$$\bar{Q}_s = \frac{Q_s}{ULm} = 2\int_0^1 \left( -\frac{d\bar{p}}{d\bar{y}} \frac{\bar{h}^3}{12\bar{\eta}} \frac{L^2}{B^2} \right) d\bar{x} \tag{5}$$

The dimensionless pivot position is determined using the following relation [44]:

$$\bar{x}_p = \frac{x_p}{L} = \frac{\int_0^1 \int_0^1 \bar{p}\, \bar{x} d\bar{x} d\bar{y}}{\int_0^1 \int_0^1 \bar{p}\, d\bar{x} d\bar{y}} \tag{6}$$

The dimensionless temperature rise is computed using the equation provided below [45]:

$$\Delta \bar{T} = \frac{m^2 \rho C_p}{\eta_0 UL} \Delta T = \frac{\bar{F}}{\bar{Q}_i} \tag{7}$$

The bearing stiffness coefficient is calculated by the following relation [46]:

$$\bar{S} = -\frac{\partial \bar{W}}{\partial \bar{h}} = -\sum_1^{Ne} \iint_{A_e} \bar{p}_h d\bar{x} d\bar{y} \tag{8}$$

where $\bar{W}$ is the dimensionless film load carrying capacity and $\bar{p}_h = \partial \bar{p} / \partial \bar{h}$

The bearing damping coefficient is found by the following expression [46]:

$$\bar{C} = -\frac{\partial \bar{W}}{\partial \dot{\bar{h}}} = -\sum_1^{Ne} \iint_{A_e} \bar{p}_{\dot{\bar{h}}} d\bar{x} d\bar{y} \tag{9}$$

where $\dot{\bar{h}} = \partial \bar{h} / \partial \bar{t}$ and $\bar{p}_{\dot{\bar{h}}} = \partial \bar{p} \Big/ \partial \dot{\bar{h}}$

The viscosity with the temperature rise of the lubricant is calculated using the following eq. [27]:

$$\eta = \eta_o e^{-\gamma (T - T_i)} \tag{10}$$

It is worth mentioning here that change in viscosity of lubricant due to film pressure remains negligible for thrust bearing case as the generated pressure is of order of MPa [27]. Normally, viscosity of oil gets influenced when pressure exists in GPa order.

### 2.1 Computation of film pressure

The following Reynolds eq. for computation of fluid pressure is employed [22]:

$$\frac{\partial}{\partial \bar{x}} \left[ \frac{\bar{h}^3}{6\bar{\eta}} \frac{\partial \bar{p}}{\partial \bar{x}} \right] + \frac{L^2}{B^2} \frac{\partial}{\partial \bar{y}} \left[ \frac{\bar{h}^3}{6\bar{\eta}} \frac{\partial \bar{p}}{\partial \bar{y}} \right] = \frac{\partial \bar{h}}{\partial \bar{x}} + 2 \frac{\partial \bar{h}}{\partial \bar{t}} \tag{11}$$

Equation (11) has been discretized employing the FEM. The discretized form is provided as follows:

$$\sum_{j=1}^{n} F_{ij}^e \bar{p}_j^e + R_i^e + \dot{R}_i^e - T_i^e = 0 \tag{12}$$

where

$$G_{ij}^e = \int_{\Omega^e} \left[ \frac{\bar{h}^3}{6\bar{\eta}} \frac{\partial N_i}{\partial \bar{x}} \frac{\partial N_j}{\partial \bar{x}} + \frac{L^2}{B^2} \frac{\bar{h}^3}{6\bar{\eta}} \frac{\partial N_i}{\partial \bar{y}} \frac{\partial N_j}{\partial \bar{y}} \right] d\bar{x} d\bar{y},$$

$$R_i^e = \int_{\Omega^e} N_i \left( \frac{\partial \bar{h}}{\partial \bar{x}} \right) d\bar{x} d\bar{y}, \dot{R}_i^e = \int_{\Omega^e} 2N_i \left( \frac{\partial \bar{h}}{\partial \bar{t}} \right) d\bar{x} d\bar{y}$$

$$T_i^e = \oint_{\Gamma^e} N_i T_n ds$$

The Gauss quadrature method is used to evaluate the above integrals. The global matrices have been found using the assembly of the element matrices.

$$\begin{bmatrix} G_{11} & G_{12} & \cdots & G_{1j} & \cdots & G_{1n} \\ G_{21} & G_{22} & \cdots & G_{2j} & \cdots & G_{2n} \\ \vdots & \vdots & \vdots & \vdots & \vdots & \vdots \\ G_{i1} & G_{i2} & \cdots & G_{ij} & \cdots & G_{in} \\ \vdots & \vdots & \vdots & \vdots & \vdots & \vdots \\ G_{n1} & G_{n2} & \cdots & G_{nj} & \cdots & G_{nn} \end{bmatrix} \begin{Bmatrix} \bar{p}_1 \\ \bar{p}_2 \\ \vdots \\ \bar{p}_i \\ \vdots \\ \bar{p}_n \end{Bmatrix} + \begin{Bmatrix} R_1 \\ R_2 \\ \vdots \\ R_i \\ \vdots \\ R_n \end{Bmatrix} + \begin{Bmatrix} \dot{R}_1 \\ \dot{R}_2 \\ \vdots \\ \dot{R}_i \\ \vdots \\ \dot{R}_n \end{Bmatrix} - \begin{Bmatrix} T_1 \\ T_2 \\ \vdots \\ T_i \\ \vdots \\ T_n \end{Bmatrix} = 0 \tag{13}$$

Equation (13) is written in short form as follows:

$$[G]\{\bar{p}\} = -\{R\} - \{\dot{R}\} + \{T\} \tag{14}$$

The above equation has two unknowns $\bar{p}$ and $T$. At the internal nodes, the flow vector $(T)$ is zero, and the pressures ( $\bar{p}$ ) are not known. But at the boundary nodes, the pressures are known (zero), and the flows are unknown. Thus, the equation (14) has as many equations as unknowns, and the solution of this equation has been obtained.

### 2.2 Film thickness relations

The film thickness relations used in the work are written as follows:

**(i) For plain/conventional pad**

$$\bar{h} = (h_1 / h_2) / (h_1 / h_2 - 1) - (x / L) \tag{15}$$

where $h_1$ and $h_2$ are inlet and outlet film thickness, respectively (refer to Fig. 1(b) for the details)

**(ii) For rectangular pocketed pad**

$$\bar{h} = (h_1 / h_2) / (h_1 / h_2 - 1) - (x / L) + \bar{h}_d \tag{16}$$

where

$$\bar{h}_d = \begin{cases} \Delta h & ;\text{if } x \le L_c; \\ & 0.5\times(B - B_r) \le y \le 0.5\times(B + B_r) \\ 0 & ;\text{otherwise} \end{cases} \tag{17}$$

**(iii) For new pocketed pad**

$$\bar{h} = (h_1 / h_2) / (h_1 / h_2 - 1) - (x / L) + \bar{h}_d \tag{18}$$

where

$$\bar{h}_d = \begin{pmatrix} \Delta h \\ \Delta h \\ 0 \end{pmatrix} \begin{matrix} ; \quad \text{if } 0 \le x \le \cot(\beta)\times 0.5\times(0.975B - B_r); \\ x\times\tan(\beta) + 0.025B \le y \le -x\tan(\beta) + 0.975B \\ ; \quad \text{if } \cot(\beta)\times 0.5\times(-B_r + 0.975B) < \theta \le L_c; \\ 0.5\times(-B_r + 0.975B) \le y \le (B_r + 0.975B)\times 0.5 \\ ; \quad \text{otherwise} \end{matrix} \tag{19}$$

## 3. SOLUTION PROCEDURE AND VALIDATION

The fluid domains for plain and new pocketed bearings have been discretised using linear quadrilateral elements as shown in Figs. 3(a) and 3(b). The number of elements used to discretize each fluid domain is 260 x 260. It has been selected by mesh independent test. The nodal pressure values are obtained by solving eq. (14) using the boundary condition that gage pressure values are zero at the edges of the pads. The eq. (14) has been solved using the Gauss elimination method. For developing the confidence in the present model based numerical results, validation of the proposed model has been done with the prior published work of the researchers [1]. In Figs. 4(a)-4(d), comparisons between the performance parameters (minimum film thickness, friction coefficient, flow ( $\bar{Q}_i$ ), and flow ratio ( $\bar{Q}_s / \bar{Q}_i$ )) of a tilting pad bearing have been presented. A good matching between both the results with ± 1% error can be seen in these figures. It is understood that the minor errors might have occurred due to different discretization techniques adopted by the authors of these two works. However, in light of the good correlation of the results, the model is considered validated and used herein for the study.

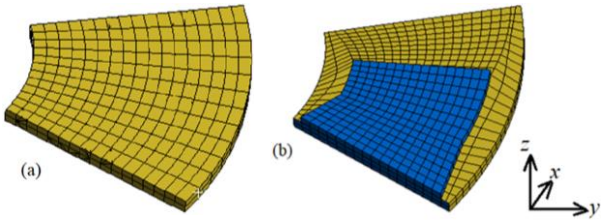


**Fig. 3.** Schematic diagrams of finite element mesh of fluid domains, (a) Film between conventional pad and runner, (b) Film between new pocketed pad and runner.

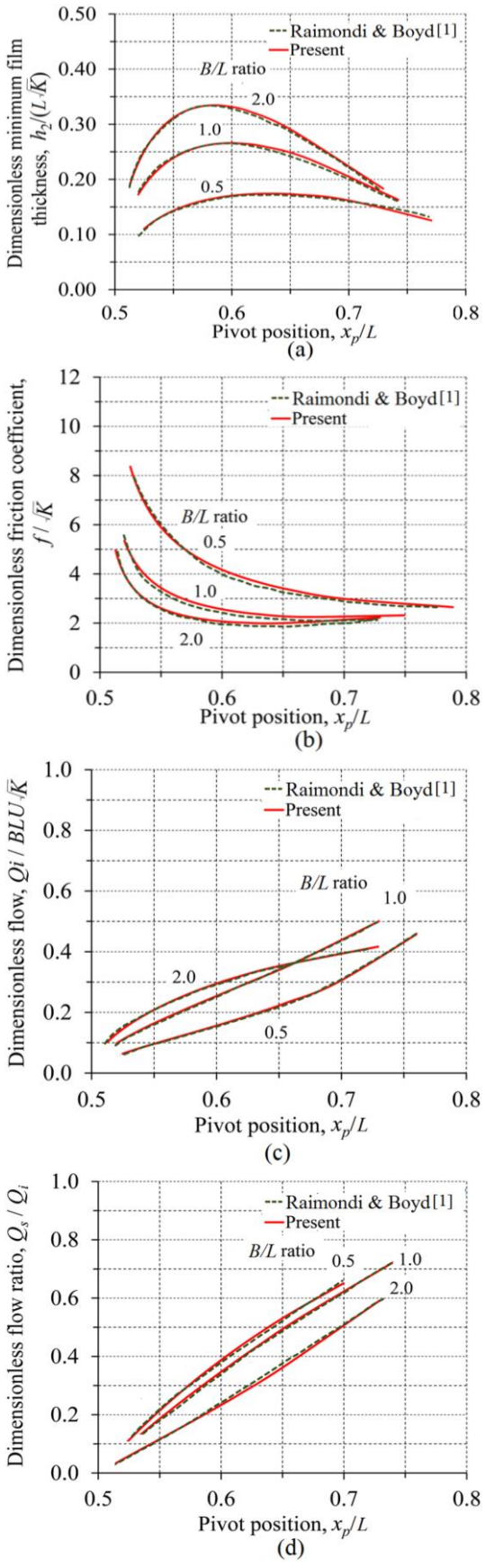


**Fig 4.** Validation of present numerical results with the work of the authors [1], (a) Dimensionless minimum film thickness, (b) Dimensionless friction coefficient, (c) Dimensionless flow, (d) Dimensionless flow ratio.

### 3.1 Validation with experimental work

In Fig. 5, the present model based computed minimum film thickness has been compared with experimentally measured minimum film thickness reported by researchers [47]. A fair agreement between the results can be seen. The small differences (an average error 5%) in the results in Fig. 5 have happened due to the consideration that all the heat produced because of oil smearing is accountable for the mean temperature increase of the fluid film.

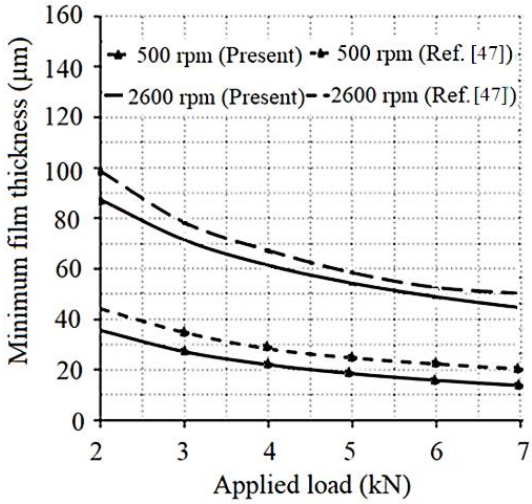


**Fig 5.** Validation of present's model based results with experimental results of the authors [47].

## 4. METHODOLOGY FOR GENERATING THE CHARTS

It is found that the load carrying capacity of tilting thrust pad bearings lie in the range corresponding to film thickness ratios ($h_1/h_2$) varying in the range of 1.05 to 6 [48].

**Step 1:** At first take ($h_1/h_2$) ratio 1.05 to calculate the film thickness at various grids in the computational domain using the equations (15)-(19).

**Step 2:** After calculation of film thickness at grid points, the dimensionless steady state pressure is found by employing Gauss elimination method in the solution of eq. (14) by employing boundary condition at the edges zero (gage pressure). It should be noted that the time dependent term on right side of eq. (14) is made zero for computing the steady state pressure in the domain.

**Step 3:** After getting the pressure at the grids, the dimensionless performance parameters are computed employing the equations (1)-(9).

**Step 4:** This process is repeated with an increment of 0.05 in $h_1/h_2$ ratio (i.e., for second time take value of this ratio as 1.10) and terminated when $h_1/h_2$ ratio reaches value of 6.

**Step 5:** The method to plot design graphs after computing the dimensionless performance parameters is provided herein.

The bearing design graphs can be presented in many ways but plotting the graphs which have the performance parameters varying with the bearing number is probably one of the good methods as this number contains bearing geometric and operating parameters. The bearing number is as follows:

$$B_T = \frac{\eta U}{WB}\left(\frac{L}{s_h}\right)^2 \tag{20}$$

where $s_h = h_1 - h_2$

Equation (19) is further expressed as below:

$$B_T = \frac{1}{\bar{W}} = \frac{\eta U}{m^2 PL} \tag{21}$$

where $P = W/(L \times B)$; $m = s_h / L$

It is worth noting here that for a tilting pad bearing, the moment of force (due to film pressure) about pivot position needs to be calculated, which prevents the choice of bearing number. Hence, in the case of tilting pad bearing, the slope ($m$) is not known. Therefore, for tilting pad case, a number known as performance number ($K$) is defined as follows:

$$K = \frac{\eta U}{PL} = B_T m^2 \tag{22}$$

Hence, equation for $m$ is as follows:

$$m = \sqrt{K/B_T} \tag{23}$$

**Step 6:** The basic design variable for a tilting pad bearing case is the pivot position. Calculate the pivot position using eq. (5).

**Step 7:** Redefine the performance variables of tilting pad bearings by inserting expression of $m$ from eq. (23) to eqs. (2), (3), (4), (5), (8) and (9) and then plot these as a function of pivot position. The method to use these plots is provided in section 5.2.

## 5. RESULTS AND DISCUSSIONS

The charts have been presented for surface profiles, namely, (a) new pocketed pad, (b) and plain pad, at three ($B/L$) ratios, i.e., 0.5, 1.0, and 2.0. In the proposed design charts, dash lines indicate the case of the plain pad; however, solid lines correspond to new micro-pocketed pad. In the charts for new pocketed pad tilting pad bearing, the solid curves have been drawn for the values of different dimensionless circumferential extents ($L_c/L$) while the values of dimensionless radial extents ($B_r/B$), pocket depth ($h_d$) and angle ($\beta$) were taken 0.7, 0.9 x $h_2$ and 15°, respectively. These values of $B_r/B$, $h_d$, and $\beta$ have been optimized employing the trial-and-error method [40].

### 5.1 Charts for new micro-pocketed tilting pad bearings

Figures (6)-(8) show the design charts for new pocketed (refer Fig. 2(b) for the geometry) and plain tilting pad thrust bearings. It is worth mentioning here that the use of these charts has been demonstrated in the solved design problem-1 given in sub-section 5.2.

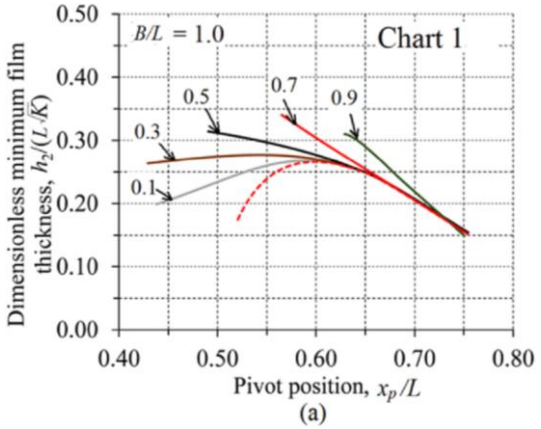


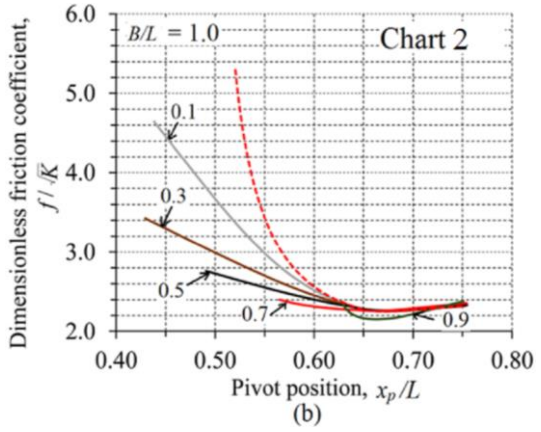

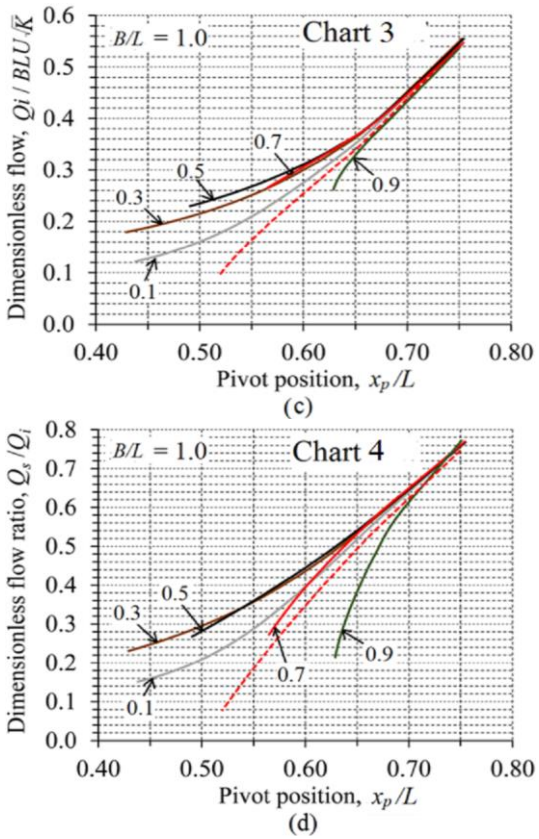


**Fig. 6**. Variation of performance parameters with pivot position for new pocketed tilting pad thrust bearing having $B/L$ = 1, (a) Dimensionless minimum film thickness, (b) Dimensionless friction coefficient, (c) Dimensionless flow, (d) Dimensionless flow ratio.

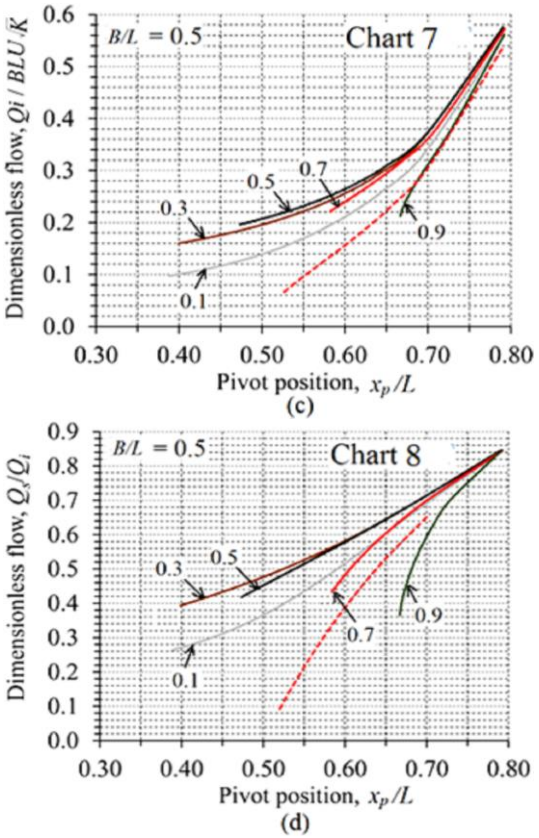


**Fig. 7.** Variation of performance parameters with pivot position for new pocketed tilting pad thrust bearing having $B/L$ = 0.5, (a) Dimensionless minimum film thickness, (b) Dimensionless friction coefficient, (c) Dimensionless flow, (d) Dimensionless flow ratio.

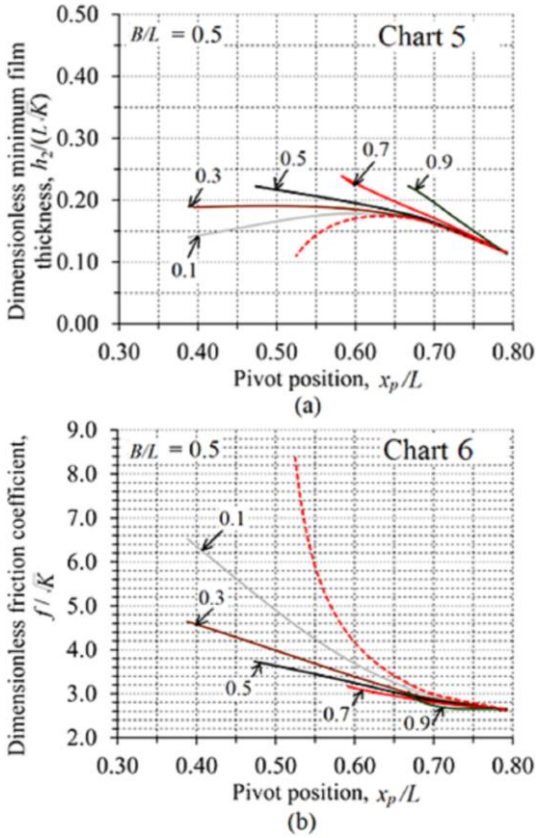


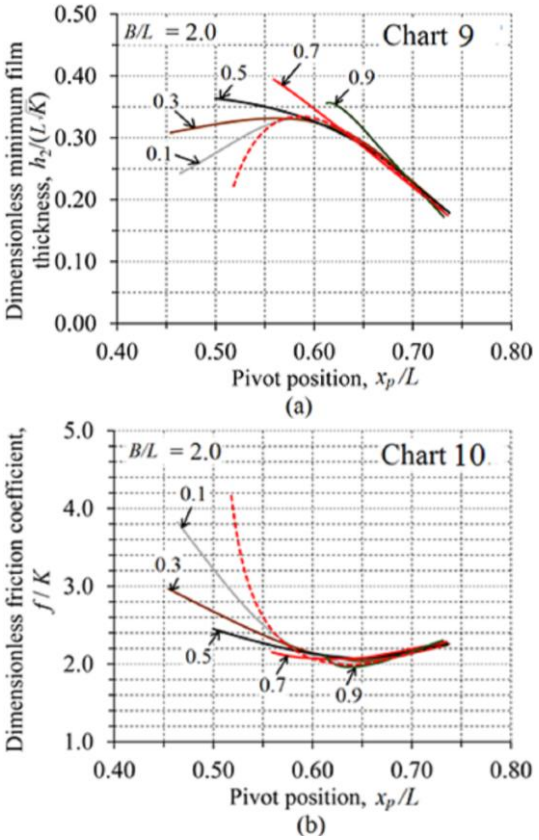

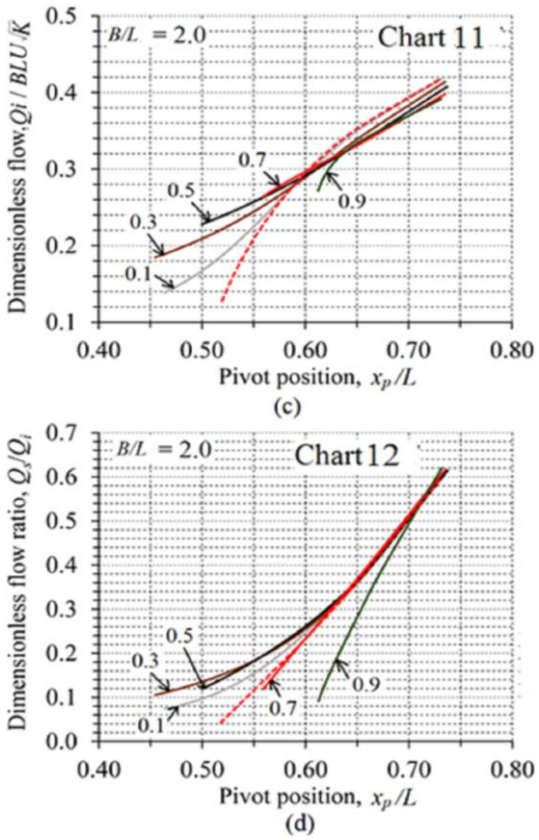


**Fig. 8.** Variation of performance parameters with pivot position for new pocketed tilting pad thrust bearing having $B/L$ = 2, (a) Dimensionless minimum film thickness, (b) Dimensionless friction coefficient, (c) Dimensionless flow, (d) Dimensionless flow ratio.

### 5.2 Design guidelines of the new micro-pocketed tilting pads

**Step-1:** List the operating parameters such as load, speed, shaft diameter, bearing application, etc.

**Step-2:** Determine inner radius ($R_1$).

The inner diameter of the bearing is kept larger than the shaft for assembly purpose, and to deliver any oil flow to the thrust bearing at its inside diameter. Typically, the diametrical clearance varies in the range 8-30 mm, corresponding to shaft diameters of 40-250 mm [49]. For finding the diametrical clearance at the intermediate values of shaft diameters, linear interpolation may be adopted.

**Step-3:** Determine outer radius ($R_2$) of bearing.

The unit load for the tilting pad varies from 1.5 - 5.0 MPa for larger size pads ($R_2$ lying in the range of 50-1500 mm). It is worth mentioning here that micro-pockets are cut on the carbon-steel pad surfaces in the absence of any coating.

Circumferential gap ($C_g$) between the two consecutive pads can be taken in the range of 10-20% of the circumferential length of a pad.

**Step-4:** Determine mean radius ($R_m$) and decide the number of pads.

- The mean radius is calculated using the relation: $R_m=(R_1+R_2)/2$
- Number of pads ($N_p$) = $2\pi R_m (1- C_g) /L$

where, $B = (R_2 - R_1)$; $B/L$=1 [initially select a finite pad (if nothing is mentioned in the problem) because it yields reasonably good performance in comparison to longer and shorter pads].

**Step-5:** Calculate surface speed of runner using the relation: $U=R_m (2\pi N / 60)$.

**Step-6:** Select the lubricant from the Lubricants handbook [50].

Guidelines: ISO VG 32 (SAE 10W), ISO VG 46 (SAE 20), and ISO VG 68 (SAE 20W) are commonly used industrial oils for the lubrication of thrust pad bearings.

Thicker oils are usually used at low speeds and thinner ones at high speeds. Initially chose ISO VG 32 oil for medium to high surface speeds and for low speeds chose higher viscous oil, i.e., ISO VG 68.

**Step-7:** Assume inlet temperature of lubricant ($T_i$). Find the viscosity of selected oil at $T_i$ using the Lubricants handbook [50].

**Step-8:** Determine the dimensionless circumferential extent of a pocket followed by the location of the pivot from the chart-1 of dimensionless minimum thickness or chart 2 of dimensionless friction coefficient (corresponding to $B/L$ ratio of 1 and case of new pocket) depending upon whether maximum load or minimum power loss is more important in the particular application.

**Step-9:** Now calculate the bearing performance number ($K$) from the given data using eq. (21).

**Step-10:** Read the dimensionless friction coefficient value from chart 2 (new pocketed case and $B/L$ ratio of 1) corresponding to the dimensionless pivot position and dimensionless circumferential extent of pocket determined in the step-8.

**Step-11:** Read dimensionless flow value from chart 3 and calculate the value of flow $Q_{i.}$

**Step-12:** Now calculate the temperature rise using the eq. (7) and then determine the new viscosity using eq. (10) or from the viscosity-temperature chart & then find the new value of $K$ corresponding to the new viscosity value.

**Step-13:** Repeat the steps (10)-(12) until the difference between values of two consecutive temperature rise becomes less than 0.5 $^0$C.

**Step-14:** Find the value of minimum film thickness ($h_2$). Is relation $(h_2)_{\text{calculated}} > 10\sqrt{\sigma_1^2+\sigma_2^2}$ hold? ($\sigma_1$ and $\sigma_2$ are surface roughness of the runner and pad, respectively). This condition ensures that bearing is working in the hydrodynamic lubrication regime. If this condition is satisfied, go to step-15, else do corrective actions such as change of lubricating oil, decrease the inlet oil temperature, improve the surface finish on the runner, etc. and then go to step-3 for iterations.

**Step-15:** Find out all performance parameters from the charts corresponding to minimum film thickness, friction coefficient, inflow, side leakage, etc.

Now, the use of these charts/graphs is demonstrated through an example.

**Problem 1:**

Design a new micro-pocketed tilting pad thrust bearing for carrying the maximum load in a steam turbine for data provided below:

Thrust load ($W$) = 50 kN,

Rotational speed of rotor= 3600 rpm,

Journal diameter of rotor = 40 mm,

The roughness of runner and pad surfaces are 0.5 μm and 1.0 μm, respectively

**Solution:**

**Step-1:**

Thrust load ($W$) = 50 kN, Rotational speed of rotor = 3600 rpm, Journal diameter of rotor = 40 mm.

**Step-2:**

Inner radius of the bearing ($R_1$) = 0.5 x 40+4=24 mm.

**Step-3:**

Taking an average unit load ($P_{\text{avg}}$) of 3 MPa on the bearing, the outer radius of bearing can be determined.

Since $P_{avg} = W/A$,

$A$=Circumferential length x (1- $C_g$ ) x width ($B$),

$B = (R_2\text{-}R_1)$ & $C_L$=0.5 x 2 x π x 0.85 x $(R_1+R_2)$

= π x 0.85 x $(R_1+R_2)$

Now $A = (R_2\text{-}R_1)$ x π x 0.85 x $(R_1+R_2)$

= $(R_2\text{^}2\text{-}R_1\text{^}2)$ x π x 0.85

Therefore, $R_2 = (R_1\text{^}2+W/(\ \pi \text{ x } 0.85 \text{ x } P_{avg}))\text{^}0.5$ which yields $R_2$ as 83 mm.

**Step-4:**

Now bearing pad width ($B$)= 83-24 = 59 mm and number of square pads with $B$=$L$ becomes 284.57/59 ≈ 5.

**Step-5:**

Surface speed ($U$) at the mid radius = π x (83+24) x 3600 x 10^-3/60=20.17 m/s

**Step-6:**

Based on the speed calculated in step-5, ISO VG32 is selected as a lubricant.

**Step-7:**

Assuming an inlet temperature of 40$^o$C for feeding of lubricant to the bearing. At the inlet temperature oil has viscosity of 0.026 Pa-s (ref. [49]).

**Step-8:**

For maximum load condition, pivot location is selected as 0.56 (Chart 1), corresponding to the dimensionless circumferential extent of 0.7 as it provides the highest minimum film thickness.

**Step-9:**

Now the steps for calculating the performance of tilting pad bearing case are as follows:

$$K = \frac{\eta U}{PL} = \frac{0.026 \times 20.17}{3 \times 10^6 \times 0.059} = 2.96 \times 10^{-6}$$

and $\sqrt{K} = 0.0017$.

**Steps-10, 11 & 12:**

The friction coefficient, inflow and temperature rise using the charts are provided below in Table 1 respectively.

**Table 1.** Iterations using charts.

| Iteration no | $K$ | $f/\sqrt{K}$ (Chart 14) | $f$ | $Q_i/(BLU\sqrt{K})$ (Chart 15) | $Q_i$ (m³/s) | $\Delta T$ (⁰C) |
|---|---|---|---|---|---|---|
| 1 | 2.96E-6 | 2.40 | 0.0041 | 0.262 | 3.16E-5 | 15.37 |
| 2 | 1.87E-6 | 2.40 | 0.0032 | 0.262 | 2.51E-5 | 15.42 |

**Step-13:**

The difference between two consecutive average temperature rise is less than 0.5 ⁰C . Hence, these iterations can be stopped here.

**Step-14:**

Using chart 1 minimum film thickness ($h_2$) = 27.14 μm

Since $(h_2)_{calculated} > 10\sqrt{0.5^2 + 1^2} = 11.11$ μm, hence go to step-15

**Step-15:**

Now all performance parameters of new pocketed bearing can be calculated and given below in Table-2.

**Table 2.** Performance parameters of new pocketed bearing.

| $h_2/(L\sqrt{K})$ | $h_2$ (μm) | $f/\sqrt{K}$ | $f$ | $Q_i/(BLU\sqrt{K})$ | $Q_i$ (m³/s) | $Q_s/Q_i$ | $Qs$ (m³/s) | $\Delta T$ (⁰C) |
|---|---|---|---|---|---|---|---|---|
| 0.341 | 27.14 | 2.40 | 0.0032 | 0.262 | 2.51E-5 | 0.275 | 6.903E-6 | 15.42 |

Figures 9(a) and 9(b) present the 3D film shape and pressure profiles for this solved problem of new pocketed pad bearings for ready reference to the readers. It can be seen from the Fig. 9(b) the maximum pressure generates towards the outlet side where the pocket ends.

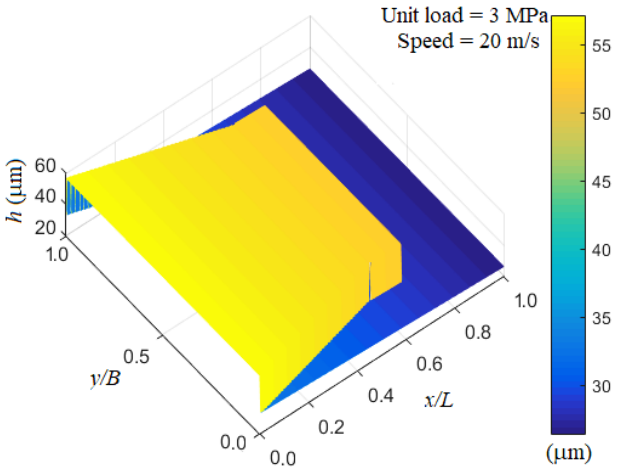


**Fig. 9a.** 3D film thickness profile for the case of solved Problem 1.

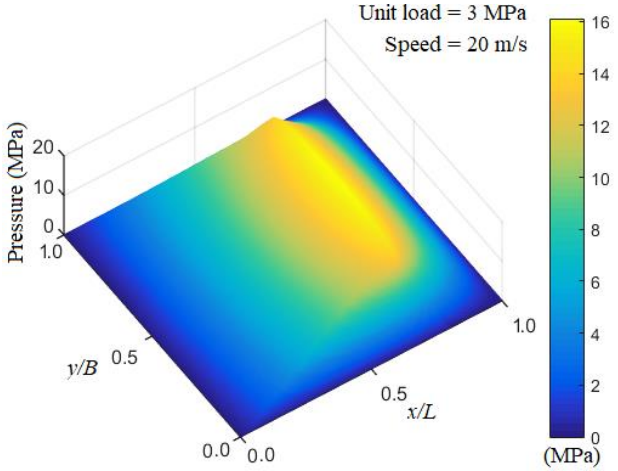


**Fig. 9b.** 3D pressure profile for the case of solved Problem 1.

### 5.3 Charts for bearing dynamic coefficients

The charts for dynamic coefficients of both pocketed & plain tilting pad bearings are presented in this subsection, and their use is also demonstrated through a numerical problem.

**Bearing dynamic coefficients charts for the new micro-pocketed tilting pad thrust bearings**

Figures 10(a)-10(f) depict the bearing dynamic coefficients for new pocketed tilting pad thrust bearings having different $B/L$ ratios.

**Problem 2:**

Determine the bearing dynamic coefficients of both the micro-pocketed pad bearings using the input parameters given in Problem -1.

**Solution:**

**Stiffness coefficient:** From chart 13, dimensionless stiffness coefficient corresponding to pivot position of 0.56 and $L_c/L$=0.7 is given as follows:

$$SK^{1.5}L/\eta UB = 6.4$$

$S$ = 6.4 x 0.0164 x 20.17/(1.87E-6)^1.5

= 8.28 x $10^8$ N/m

**Damping coefficient:** From chart 16, dimensionless damping coefficient corresponding to pivot position of 0.56 and $L_c/L$=0.7 is given as follows:

$$\bar{C}K^{1.5}/\eta B = 4.5$$

Therefore,

$C$ = 4.5 x 0.0164 x 0.059/(1.87 E-6)$^{1.5}$

= 1.70x $10^6$ N-s/m

### 5.4 Proposed interpolation relation

If the value of $B/L$ lies between 0.5 and 2.0 (i.e., 0.5< $B/L$ <2.0), then the following interpolation formula can be used to calculate the performance parameters of the bearings:

$$Y = (8/3)(1-B/L)(1-0.5B/L)Y_{0.5} - 2(1-2B/L)(1-0.5B/L)Y_{1.0} + (1/3)(1-B/L)(1-2B/L)Y_{2.0}$$

Where $Y$ is a performance parameter at the required $B/L$ ratio

$Y_{0.5}$= performance parameter corresponding to $B/L$ = 0.5

$Y_{1.0}$ = performance parameter corresponding to $B/L$ = 1.0

$Y_{2.0}$= performance parameter corresponding to $B/L$ = 2.0

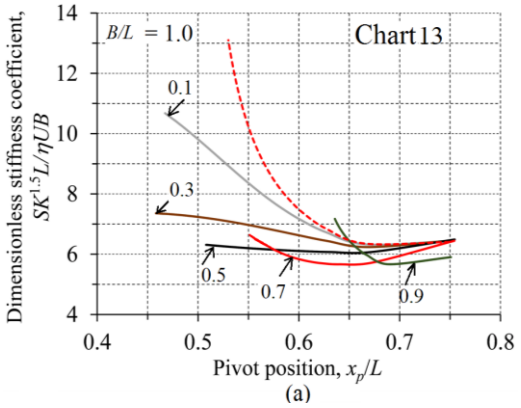


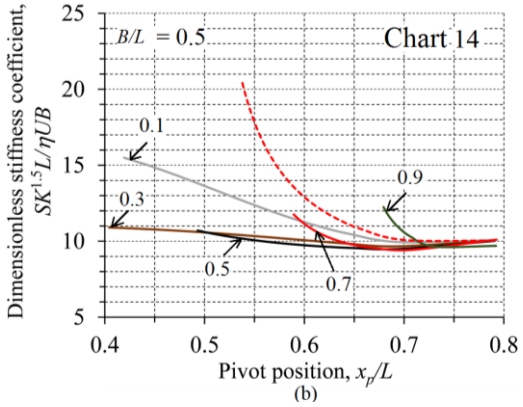


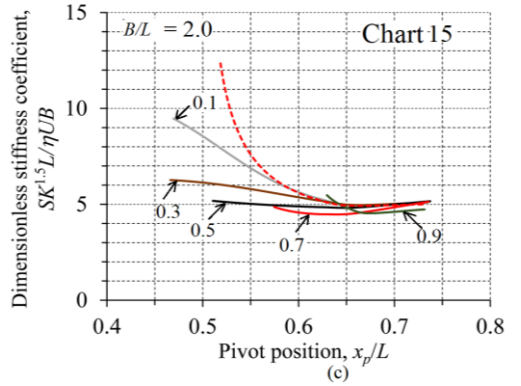


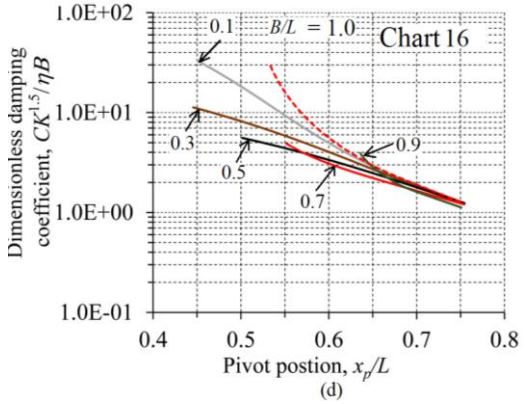

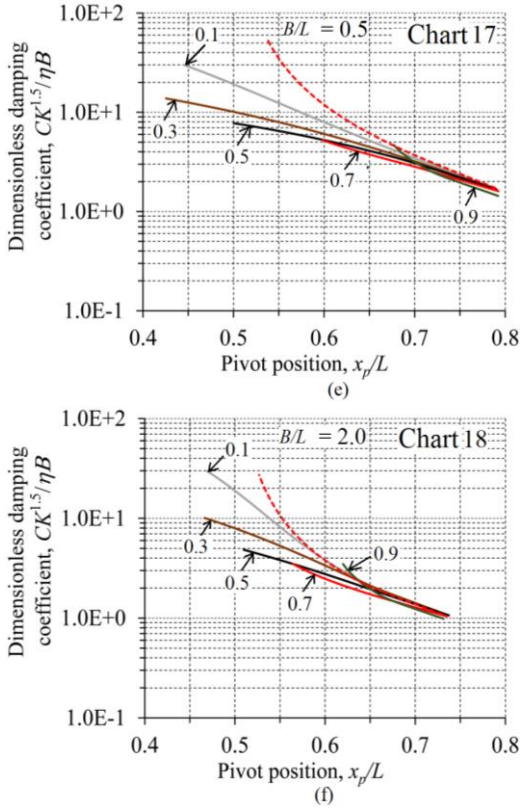


**Fig. 10.** Changes in bearing dynamic coefficients with pivot position for new pocketed tilting pad thrust bearing, (a) Dimensionless stiffness coefficient for $B/L$=1, (b) Dimensionless stiffness coefficient for $B/L$=0.5, (c) Dimensionless stiffness coefficient for $B/L$=2, (d) Dimensionless damping coefficient for $B/L$=1, (e) Dimensionless damping coefficient for $B/L$=0.5, (f) Dimensionless damping coefficient for $B/L$=2.

### 5.5 Comparison between the performances of tilting pocketed and plain pads

This subsection presents the comparison of the performance of tilting pocketed pads.

#### Comparison between rectangular, new micro-pocketed and plain pads

Figure 11(a) presents the comparison of the dimensionless maximum-minimum film thickness of rectangular, new, and plain pads at different $B/L$ ratios with performance number ($K$) (which is related to predefined or applied load). It can be seen that both the micro pocketed pads achieve higher min film thickness compared to plain case. New pocketed and rectangular pocketed pads can have up to 37.4% and 28.23% higher film thickness for $B/L$ =0.5. Moreover, a maximum decrease up to 14.3% and 7.7% can be achieved with the new and rectangular pocketed pads, respectively (Fig. 11(b)). It can also be noticed from Fig. 11(a) that the new pocketed pad attains up to 7.70 % better minimum film thickness as compared to the rectangular-shaped pocketed case. It is also seen from this figure that as the $B/L$ ratio increases from 0.5 to 2, the variation between the min film thickness of both micro-pocketed pads decreases. This occurs because with an increase in $B/L$ ratio, the circumferential length of a pad reduces, which diminishes the geometrical shape effect of the trapezoidal part of the new pocketed pad. A reduction of up to 7% in friction coefficient can be achieved with new- pocketed pad compared to rectangular-shaped pocketed pad for $B/L$ =0.5 as observed from Fig. 11(b).

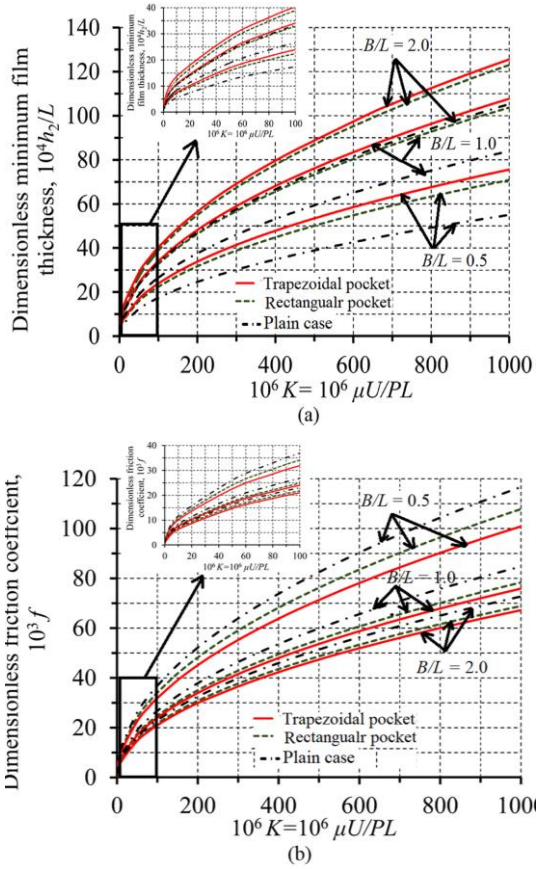


**Fig. 11.** (a) Comparison of minimum film thickness among rectangular, new micro-pocketed & plain pads, (b) Comparison of friction coefficient among rectangular, new micro-pocketed & plain pads.

As it can be noticed from the above figures that both the micro-pocketed pads achieved better performance than the plain pad. The reason can be explained with the help of Fig. 12.

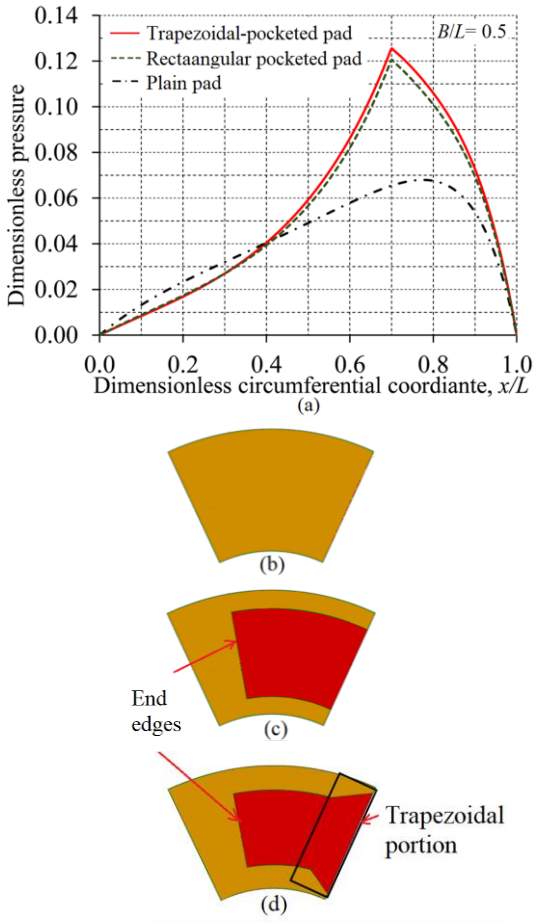


**Fig. 12.** (a) Film-pressure profiles (at mid-radius plane) comparison of both the micro-pocketed pads with pressure profile of plain pad, (b) Schematic of plain pad, (c) Rectangular-shaped pocketed pad (d) New-pocketed pad.

In Fig. 12(a), comparisons of pressure profiles of the plain pad (Fig. 12(b)) have been shown with both micro-pocketed pads (Fig. 12(c) and 12(d)). It can be seen from Fig. 12(a) that both the micro-pockets develop higher pressure than the plain pad. This is due to the formation of micro-dams at the end edges of both the micro-pockets (see Fig. 12(c) and 12(d))) which restrict the flow of lubricant in the circumferential direction leading to the generation of higher pressure than the plain pad. Moreover, it is also noticed from Fig. 12(a) that pressure in the case of the new pocketed pad is higher than the rectangular pocket. This happens because the trapezoidal portion (see Fig. 12(d)) of the new pocketed pad gradually restricts the flow of lubricant in the inlet zone as compared to the inlet region of the rectangular pocketed pad, which leads to the generation of higher pressure in new pocketed pad case.

## 5. CONCLUSIONS

The analysis presented in this paper revealed that the proposed new micro-pocketed pad performed better in comparison to the conventional rectangular pocketed and conventional (plain) pads. Up to 37.4% and 7.7% increase in minimum film thickness and 14.3% & 7% decrease in friction coefficient have been found as compared to the conventional and rectangular pocketed pads, respectively. Based on the work presented in this paper for the proposed new micro-pocketed tilting thrust pad bearing, the design charts for the rapid calculation of minimum film thickness, friction coefficient, inflow, side flow, bearing stiffness coefficient and damping coefficients, have been provided. Moreover, two solved problems have also been provided demonstrating the use of proposed approach of design.

## Acknowledgement

Authors recognize the HPC, Baadal, and CAGIL lab computational facilities of IIT Delhi, India. The first author is thankful to MHRD for providing scholarship to carry out the Ph.D. at this institute.

## REFERENCES

[1] A.A. Raimondi, J. Boyd, *Applying Bearing Theory to the Analysis and Design of Pad-Type Bearings*, Journal of Fluids Engineering, vol. 77, iss. 3, pp. 287-309, 1955, doi: 10.1115/1.4014331

[2] M.M. Khonsari, J.Y. Jang, *Thermohydrodynamic Design Charts for Slider Bearing,* Journal of Tribology, vol. 119, iss. 4, pp. 733-740, 1997, doi: 10.1115/1.2833878

[3] M. Arghir, N. Roucou, M. Helene, J. Frene, *Theoretical Analysis of the Incompressible Laminar Flow in a Macro-Roughness Cell*, Journal of Tribology, vol. 125, iss. 2, pp. 309-318, 2003, doi: 10.1115/1.1506328

[4] G.C. Buscaglia, I. Ciuperca, M. Jai, *The Effect of Periodic Textures on the Static Characteristics of Thrust Bearings*, Journal of Tribology, vol. 127, iss. 4, pp. 899–902, 2005, doi: 10.1115/1.2033896

[5] M.B. Dobrica, M. Fillon, *About the Validity of Reynolds Equation and Inertia Effects in Textured Sliders of Infinite Width*, Proceedings of the Institution of Mechanical Engineers, Part J: Journal of Engineering Tribology, vol. 223, iss. 1, pp. 69-78, 2009, doi: 10.1243/13506501JET433

[6] S. Cupillard, M.J. Cervantes, S. Glavatskih, *Pressure Build-up Mechanism in a Textured Inlet of a Hydrodynamic Contact*, Journal of Tribology, vol. 130, iss. 2, pp. 1-10, 2008, doi: 10.1115/1.2805426

[7] M.D. Pascovici, T. Cicone, M. Fillon, M.B. Dobrica. *Analytical Investigation of a Partially Textured Parallel Slider*, Proceedings of the Institution of Mechanical Engineers, Part J: Journal of Engineering Tribology, vol. 223, iss. 2, pp. 151-158, 2009, doi: 10.1243/13506501JET470

[8] J. Han, L. Fang, J. Sun, S. Ge, *Hydrodynamic Lubrication of Micro Dimple Textured Surface using Three-Dimensional CFD*, Tribology Transactions, vol. 53, iss. 6, pp. 860-870, 2010, doi:10.1080/10402004.2010.496070

[9] V.G. Marian, D. Gabriel, G. Knoll, S. Filippone, *Theoretical and Experimental Analysis of a Laser Textured Thrust Bearing*, Tribology Letters, vol. 44, iss. 3, pp. 335-343, 2011, doi: 10.1007/s11249-011-9857-8

[10] Y. Henry, J. Bouyer, M. Fillon, *An Experimental Analysis of the hydrodynamic contribution of textured thrust bearings during steady-state operation: A comparison with the untextured parallel surface configuration*, Proceedings of the Institution of Mechanical Engineers, Part J: Journal of Engineering Tribology, vol. 229, iss. 4, pp. 362-375, 2015, doi: 10.1177/1350650114537484

[11] J.C. Atwal, R.K. Pandey, *Film Thickness and Friction Investigations in a Fluid Film Thrust Bearing Employing New Conceived Micro-Texture on Pads*, Journal of Tribology, vol. 143, iss. 6, pp. 1-13, 2020, doi:10.1115/1.4048500

[12] J.C. Atwal, R.K. Pandey, *Performance Analysis of Thrust Pad Bearing using Micro-Rectangular Pocket and Bionic Texture*, Proceedings of the Institution of Mechanical Engineers, Part J: Journal of Engineering Tribology, vol. 235, iss. 6, pp. 1232-1250, 2020, doi: 10.1177/1350650120940076

[13] J.C. Atwal, R.K. Pandey, *Synergistic Effect of Pocket and Bionic Texture on the Performance Behaviours of Thrust Pad Bearing*, in R. Kumar, V.S. Chauhan, M. Talha, H. Pathak (Ed.): Machines, Mechanism and Robotics, Springer, Singapore, pp. 1143-1155, 2021, doi:10.1007/978-981-16-0550-5_109

[14] I. Etsion, G. Halperin, V. Brizmer, Y. Kligerman. *Experimental Investigation of Laser Surface Textured Parallel Thrust Bearings*, Tribology Letters, vol. 17, iss. 2, pp. 295-300, 2004, doi: 10.1023/B:TRIL.0000032467.88800.59

[15] U. Sudeep, N. Tandon, R.K. Pandey, *Performance of Lubricated Rolling/Sliding Concentrated Contacts with Surface Textures: A Review*, Journal of Tribology, vol. 137, iss. 3, pp. 031501, 2015, doi: 10.1115/1.4029770

[16] D. Gropper, L. Wang, T.J. Harvey, *Hydrodynamic Lubrication of Textured Surfaces: A Review of Modeling Techniques and Key Findings*, Tribology International, vol. 94, pp. 509-529, 2016, doi: 10.1016/j.triboint.2015.10.009

[17] C. Gachot, A. Rosenkranz, S.M. Hsu, H.L. Costa, *A Critical Assessment of Surface Texturing for Friction and Wear Improvement*, Wear, vol. 372-373, pp. 21-41, 2017, doi: 10.1016/j.wear.2016.11.020

[18] A. Atulkar, R.K. Pandey, P.M.V. Subbarao, *Role of Textured Piston Rings/Liners in Improving the Performance Behaviours of IC Engines: A Review with Vital Findings*, Surface Topography: Metrology and Properties, vol. 9, iss. 2, pp. 1-9, 2021, doi:10.1088/2051-672X/ac0a36

[19] A. Atulkar, R.K. Pandey, P.M.V. Subbarao, *Performance Analysis of Two-Dimensional Section of Partially Textured Piston Ring with Cavitation Boundary Conditions*, Surface Topography: Metrology and Properties, vol. 9, iss.2, pp. 1-17, 2021, doi: 10.1088/2051-672X/abfd05

[20] M.R. Pattnayak, R.K. Pandey, J.K. Dutt, *Performance Improvement of an Oil-Lubricated Journal Bearing using Bionic-Textures Fused Micro-Pockets*, Journal of Tribology, vol. 144, iss. 4, pp. 1-16, 2022, doi: 10.1115/1.4051654

[21] J. Han, L. Fang, J. Sun, S. Ge, *Hydrodynamic Lubrication of Micro Dimple Textured Surface Using Three-Dimensional CFD*, Tribology Transactions, vol, 53, iss. 6, pp. 860-870, 2010, doi: 10.1080/10402004.2010.496070

[22] H. Yu, X. Wang, F. Zhou, *Geometric Shape Effects of Surface Texture on the Generation of Hydrodynamic Pressure between Conformal Contacting Surfaces*, Tribology Letters, vol. 37, iss. 2, pp. 123-130, 2010, doi: 10.1007/s11249-009-9497-4

[23] S. Yuan, W. Huang, X. Wang, *Orientation Effects of Micro-Grooves on Sliding Surfaces*, Tribology International, vol. 44, iss. 9, pp. 1047-1054, 2011, doi: 10.1016/j.triboint.2011.04.007

[24] H. Yu, H. Deng, W. Huang, X. Wang, *The Effect of Dimple Shapes on Friction of Parallel Surfaces,* Proceedings of the Institution of Mechanical Engineers, Part J: Journal of Engineering Tribology, vol. 225, iss. 8, pp. 693-703, 2011, doi: 10.1177/1350650111406045

[25] H. Yu, W. Huang, X. Wang, *Dimple Patterns Design for Different Circumstances*, Lubrication Science, vol. 25, iss. 2, pp. 67-78, 2013, doi: 10.1002/ls.168

[26] J. Ji, Y. Fu, Q. Bi, *The Influence of Partially Textured Slider with Orientation Ellipse Dimples on the Behavior of Hydrodynamic Lubrication*, Industrial Lubrication and Tribology, vol. 66, iss. 2, pp. 161-167, 2014, doi:10.1108/ILT-11-2011-0087

[27] J.C. Atwal, R.K. Pandey, *Performance Improvement of Water-Lubricated Thrust Pad Bearing Operating with the Turbulent Flow using a New Micro-Pocket Design*, Tribology International, vol. 154, 2021, doi: 10.1016/j.triboint.2020.106738

[28] J. C. Atwal, R. K. Pandey, *Influence of New Surface Micro-Structures on the Performance Behaviours of Fluid Film Tilting Pad Thrust Bearings*, Proceedings of the Institution of Mechanical Engineers, Part C: Journal of Mechanical Engineering Science, vol. 236, iss. 6, pp. 3111-3134, 2021, doi: 10.1177/09544062211030972

[29] C.I. Papadopoulos, L. Kaiktsis, M. Fillon, *Computational Fluid Dynamics Thermohydrodynamic Analysis of Three-Dimensional Sector-Pad Thrust Bearings with Rectangular Dimples*, Journal of Tribology, vol. 136, iss. 1, pp. 1-11, 2014, doi: 10.1115/1.4025245

[30] M. B. Dobrica, M. Fillon, M. D. Pascovici, T. Cicone, *Optimizing Surface Texture for Hydrodynamic Lubricated Contacts using a Mass-Conserving Numerical Approach,* Proceedings of the Institution of Mechanical Engineers, Part J: Journal of Engineering Tribology, vol. 224, iss. 8, pp. 737-750, 2010, doi: 10.1243/13506501JET673

[31] C. I. Papadopoulos, P. G. Nikolakopoulos, L. Kaiktsis, *Geometry Optimization of Textured Three-Dimensional Micro-Thrust Bearings* Journal of Tribology, vol. 133, iss. 4, pp. 041702, 2011, doi: 10.1115/1.4004990

[32] X. Wang, J. Wang, B. Zhang, W. Huang, *Design Principles for the Area Density of Dimple Patterns,* Proceedings of the Institution of Mechanical Engineers, Part J: Journal of Engineering Tribology, vol. 229, iss. 4, pp. 538-546, 2015, doi: 10.1177%2F1350650114531939

[33] R. Rahmani, A. Shirvani, H. Shirvani, *Optimization of Partially Textured Parallel Thrust Bearings with Square-Shaped Micro-Dimples*, Tribology Transactions, vol. 50, iss. 3, pp. 401–406, 2007, doi: 10.1080/10402000701429261

[34] C. Shen, M. M. Khonsari, *Numerical Optimization of Texture Shape for Parallel Surfaces under Unidirectional and Bidirectional Sliding*, Tribology International, vol. 82, pp. 1-11, 2015, doi: 10.1016/j.triboint.2014.09.022

[35] G. Fu, A. Untaroiu, *An Optimum Design Approach for Textured Thrust Bearing with Elliptical-Shape Dimples Using Computational Fluid Dynamics and Design of Experiments Including Cavitation,* Journal of Engineering for Gas Turbines and Power, vol. 139, iss. 9, pp. 1-9, 2017, doi: 10.1115/1.4036188

[36] S. Aggarwal, R. K. Pandey, *Performance Investigation of Micro-Pocketed Textured Pad Thrust Bearing*, Industrial Lubrication and Tribology, vol. 70, iss. 8, pp. 1388-1395, 2018, doi: 10.1108/ILT-10-2017-0302

[37] D. Gropper, T.J. Harvey, L. Wang, *A Numerical Model for Design and Optimization of Surface Textures for Tilting Pad Thrust Bearings*, Tribology International, vol. 119, pp. 190-207, 2018, doi: 10.1016/j.triboint.2017.10.024

[38] D.G. Fouflias, A.G. Charitopoulos, C.I. Papadopoulos, L. Kaiktsis, M. Fillon, *Performance Comparison Between Textured, Pocket, and Tapered-Land Sector-Pad Thrust Bearings using Computational Fluid Dynamics Thermohydrodynamic Analysis*, Proceedings of the Institution of Mechanical Engineers, Part J: Journal of Engineering Tribology, vol. 229, iss. 4, pp. 376-397, 2015, doi: 10.1177/1350650114550346

[39] S. Aggarwal, R. K. Pandey, *Frictional And Load-Carrying Behaviours Of Micro-Textured Sector Shape Pad Thrust Bearing Incorporating The Cavitation And Thermal Effects*, Lubrication Science, vol. 29, iss. 4, pp. 255-277, 2017, doi: 10.1002/ls.1367

[40] V. Zouzoulas, C.I. Papadopoulos, *3-D Thermohydrodynamic Analysis of Textured, Grooved, Pocketed and Hydrophobic Pivoted-Pad Thrust Bearings*, Tribology International, vol. 110, pp. 426-440, 2017, doi: 10.1016/j.triboint.2016.10.001

[41] R.K. Sharma, R.K. Pandey, *Influence of Surface Profile on Slider Bearing Performance. International Journal of Surface Science*, vol. 2, no. 3-4, pp. 265-280, 2008, doi: 10.1504/IJSURFSE.2008.020498

[42] R.K. Sharma, R.K. Pandey, *Thermohydrodynamic Analysis of Infinitely Wide Cycloidal Profiled Pad Thrust Bearing with Rough Surface, and a Comparison to Plane Profiled Pad*, Lubrication Science, vol. 20, iss. 3, pp. 183-203, 2008, doi: 10.1002/ls.55

[43] R.K. Sharma, R.K. Pandey, *Experimental Studies of Pressure Distributions in Finite Slider Bearing with Single Continuous Surface Profiles on the Pads*, Tribology International, vol. 42, iss. 7, pp. 1040-1045, 2009, doi: 10.1016/j.triboint.2009.02.010

[44] W.W. Ni, C.L. Griffiths, D. J. Bartholme, R. Hergert, *Two-Dimensional Analytical Analysis of Fluid Film Thickness on Pivoting Tilting Pad Bearing,* SAE International, vol. 116, pp. 1040-1046, 2007, doi: 10.4271/2007-01-4140

[45] D.V. De Pellegrin, D.J. Hargreaves, *an isoviscous, isothermal model investing the influence of hydrostatic recesses on a spring supported tilting pad thrust bearing*, Tribology International, vol. 51, pp. 25-35, 2012, doi: 10.1016/j.triboint.2012.02.008

[46] S.C. Sharma, S.K. Yadav, *A comparative study of full and partial textured hybrid orifice compensated circular thrust pad bearing system,* Tribology International, vol. 95, pp. 170-180, 2016, doi: 10.1016/j.triboint.2015.11.008

[47] A. Dadouche, M. Fillon, J.C. Bligoud, *Experiments on thermal effects in a hydrodynamic thrust bearing*, Tribology International, vol. 33, iss. 3-4, pp. 167-174, 2000, doi: 10.1016/S0301-679X(00)00023-2

[48] A.A. Raimondi, *An Adiabatic Solution for the Finite Slider Bearing (L/B= 1),* ASLE Transactions, vol. 9, iss. 3, pp. 283-298, 1966, doi: 10.1080/05698196608972145

[49] M.M. Khonsari, E.R. Booser, *Applied Tribology: Bearing Design and Lubrication*, New York: John Wiley & Sons, 2008.

[50] G.E. Totten, R.J. Shah, D.R. Forester, *Fuels, and Lubricants Handbook: Technology, Properties, Performance, and Testing*, ASTM International, 2003.